Trajectory Optimization in User-Centric Distributed Massive MIMO Systems Enabled by UAV Swarms

Daynara D. Souza, Marx M. M. Freitas, André L. P. Fernandes, Pedro H. J. Nardelli, *Senior Member, IEEE,* Daniel Benevides da Costa, *Senior Member, IEEE,* André Mendes Cavalcante, *Member, IEEE,* and João C. Weyl Albuquerque Costa, *Senior Member, IEEE*

***Abstract*—User-centric (UC) distributed massive multiple-input multiple-output (D-mMIMO), commonly called cell-free mMIMO, is an important technology to ensure a more uniform coverage as well as higher spectral and energy efficiencies in next generation communication systems. This paper investigates the performance of UC D-mMIMO systems enabled by a swarm of unmanned aerial vehicles (UAVs). Specifically, it presents a comprehensive study on UAVs' deployment and trajectory optimization as aerial transmission and reception points (TRPs) of D-mMIMO systems, considering systems composed solely of aerial TRPs and those formed combining aerial and terrestrial TRPs. Moreover, user equipment (UE) mobility is modeled using a discrete-time Markov chain, and a novel approach to heuristically optimize the positions of aerial TRPs is proposed, one that considers the continuous movement of UEs in the coverage area. The proposed approach optimizes each UAV's three-dimensional location under a time discretization framework, with the positioning of the UAVs being adjusted periodically, allowing for iterative trajectory optimization to improve the UEs' spectral efficiency (SE) performance. Simulation results reveal that the proposed UAV trajectory optimization allows for significant SE improvement, especially for a low UE density scenario. Specifically, comparing the proposed method with a fixed position setup, up to 47.84% increase on average SE is achieved.**

***Index Terms*—Aerial TRPs, cell-free massive MIMO networks, computational complexity, deployment and trajectory optimization, user-centric approach, unmanned aerial vehicles.**

I. Introduction

User-centric (UC) distributed massive multiple-input multiple-output (D-mMIMO) networks, also called cell-free (CF)-mMIMO networks, are envisioned as promising technologies for next-generation wireless networks. In D-mMIMO systems, many transmission and reception points (TRPs) are spread out in the coverage area, each equipped with one or more antennas [1], [2]. The users' equipment (UEs) share the same time-frequency resources, and each UE is served by a specific subset of TRPs defined by their needs and requirements, giving rise to UC concept. These networks stand out for their high spectral efficiency (SE), reduced susceptibility to blocking and shadowing, and uniform performance among UEs [3], [4].

Along with these advantages, new challenges also arise. Problems related to power control, signal precoding, resource allocation, decoding strategies, and interference management are critical issues. Furthermore, to achieve a scalable and efficient D-mMIMO system, the complexity and resource requirements for each TRP must remain finite when the number of UEs tends to infinity [5]–[7].

Nevertheless, deploying a terrestrial infrastructure might be neither cost-effective nor feasible in practical cases, such as complex terrains, private areas, or remote areas. Also, in some occasions, terrestrial wireless networks may be disrupted or not be available due to natural disasters, power outages, maintenance, and other factors. In those situations, aerial communication systems based on unmanned aerial vehicles (UAVs) are regarded as a promising new paradigm to facilitate fast and highly flexible deployment of communication infrastructure due to their high maneuverability [2], [8]. UAVs can be regarded as a reusable aircraft designed to operate without onboard people, which can be controlled remotely or programmed to fly autonomously [9].

For each UAV, there are physical constraints on weight, size, and energy consumption, that limit the amount of onboard equipment to be carried, including the number of TRP antennas. Nonetheless, the gains of employing a large number of antennas can still be achieved by the UAVs cooperation as the TRPs of a UC D-mMIMO system, even with a small number of antennas per TRP. In this case, the UAVs operate like a cooperative swarm that maintains and adjusts their formation to engage in collaborative missions by sharing their goals and individual energy and data resources. The UAV swarms can be particularly useful in scenarios where the wireless network's dynamic nature is taken into account, such as when the UEs' positions are constantly changing due to their mobility. The maneuverability of UAVs allows for their positions to be adjusted according to the current state of the system, and their trajectories can change along with the movement of UEs.

This work was partly supported by the Innovation Center, Ericsson Telecomunicações Ltda., Brazil, by the National Council for Scientific and Technological Development (CNPq) and by the Coordination for the Improvement of Higher Education Personnel (CAPES). This paper is also partly supported by Research Council of Finland via: (a) X-SDEN project n.349965 (b) EnergyNet Fellowship n.321265/n.328869 and (c) ECO-NEWS project n.358928, and Jane and Aatos Erkko Foundation Via STREAM project.

Daynara D. Souza, Marx M. M. Freitas, André L. P. Fernandes, and João C. Weyl Albuquerque Costa are with the Applied Electromagnetism Laboratory, Federal University of Pará - UFPA, Belém, PA, 66075-110 Brazil (e-mail:{daynara;marx;andrelpf;jweyl}@ufpa.br).

Pedro H. J. Nardelli and Daynara D. Souza are with Lappeenranta-Lahti University of Technology, Lappeenranta, 53850 Finland (e-mail:{ pedro.nardelli;daynara.dias.souza}@lut.fi).

Daniel Benevides da Costa is with the Department of Electrical Engineering, King Fahd University of Petroleum & Minerals (KFUPM), Dhahran 31261, Saudi Arabia (email: danielbcosta@ieee.org).

André Mendes Cavalcante is with Ericsson Research, Ericsson Telecomunicações Ltda., Indaiatuba, SP, 13337-300 Brazil (e-mail: andre.mendes.cavalcante@ericsson.com).

In this context, implementing a swarm of UAVs working collaboratively as TRPs for UC D-mMIMO networks needs to be investigated appropriately, and several operational challenges are required to be addressed, such as data transmission in areas where a traditional network is not available or unable to support the demands. Additionally, the horizontal positions, altitudes, and trajectories of UAVs need to be optimized to adapt to the continuous movement of UEs.

A. Literature Review

Recently, the integration of UAVs into wireless communication systems has been proposed to enhance network coverage, capacity, and energy efficiency. The case of D-mMIMO systems enabled by a collaborative UAV swarm has not yet been fully investigated in detail. In the works that leverage UAVs and D-mMIMO networks, UAVs primarily serve as either aerial TRPs (base stations) [10]–[19] or aerial mobile UEs [20], [21]. In what follows, we provide insights into the latest works that leverage UAVs as TRPs of D-mMIMO communication networks, pointing out their strengths and weaknesses.

In [10], it was introduced a framework for radio-frequency energy harvesting that combines D-mMIMO, UAVs, and reconfigurable intelligent surfaces. Such an innovative approach aims to provide a seamless energy source to remote Internet of Things (IoT) devices, reducing the required infrastructure of a high-density IoT network. However, it is noteworthy that the framework primarily emphasizes energy harvesting, with SE as a secondary objective. This approach makes sense given that IoT devices generally require low bandwidth. Moreover, the work lacks optimization for positions and trajectories of UAVs.

In [11], the authors proposed the utilization of high-amplitude platforms (HAPs) as a central processing unit (CPU) to aggregate signals from UAVs through Terahertz wireless fronthaul links. The study provided a promising deployment scheme to increase the UEs' rates. However, it lacked optimization of UAVs' positions and heights, focusing on the power optimization aspects of the system. In contrast, [12] did not focus on HAPs, but it optimized the altitude and horizontal coordinates of UAVs to maximize the UEs' downlink (DL) rates. Despite this, the latter study overlooked factors such as UEs mobility, trajectory optimization, and the possible variation of each UAV's height. In addition, it assumed the Rayleigh fading model, with the effect of line-of-sight (LoS) and non-line-of-sight (NLoS) propagation used only to calculate the average channel gain. Lastly, it only analyzed the performance of conjugate beamforming, also called maximum ratio (MR) precoding.

In [13], an investigation of uplink (UL) communication in D-mMIMO networks utilizing UAVs as flying base stations was performed. The study primarily focused on an algorithmic approach based on asymptotic signal-to-interference-plus-noise ratio (SINR) expressions for a high number of UEs to perform a deployment optimization that maximizes the UEs' UL rates. In [14], the impact of the imperfect wireless fronthaul link between UAVs and CPU was taken into account to evaluate the system's SE, allowing a more robust deployment optimization. A deeper look at possible UAV deployment strategies for D-mMIMO was presented in [15]. Despite this, [13]–[15] neglected UEs mobility and trajectory optimization.

Furthermore, [16] proposed a hybrid system alternating between UAV swarms and satellites, focusing on radio resource allocation. However, the assumption of an arbitrarily given UAV trajectory limits the applicability of the proposed solution. This was addressed by the study in [17], which proposed a trajectory optimization for the same scenario. However, both works relied on scenarios that leverage hybrid UAV and satellite systems to provide service for remote IoT devices. Therefore, they did not tackle the issue of trajectory optimization considering the UEs mobility.

In [18], the deployment of UAVs in areas without terrestrial infrastructure was explored, extending wireless resources to numerous service providers. However, the scenario in the work was a conventional cellular network instead of a UC D-mMIMO system. Moreover, the term "cell-free" that traditionally is used for UC D-mMIMO was actually used to refer to an area without cell-based internet access. Similarly, another work with the denomination "cell-free" without connection to UC D-mMIMO systems was presented in [19], where each UE was served by one UAV and had exclusive time-frequency resources.

Finally, in [20], [21], it was assumed that UAVs are the mobile UEs of the UC D-mMIMO system. In [20], power control and security aspects were investigated, while [21] evaluated whether the system can support UAV communications in the presence of interfering ground UEs. Although their proposals are an interesting line of research, they follow a different investigation scenario than our work.

In summary, while the integration of UAVs into D-mMIMO communication systems shows immense promise for enhancing wireless networks, current research often neglects crucial aspects such as UEs mobility, trajectory optimization, and heterogeneous deployment scenarios. Addressing these limitations is essential for realizing the full potential of UAV-enabled D-mMIMO communication systems in future wireless networks.

B. Contributions

By filling out some gaps that exist in the literature, the primary objective of this paper is to formulate strategies for deployment and trajectory optimization of UAVs within the context of UC D-mMIMO networks, where a swarm of UAVs cooperatively serve the UEs as aerial TRPs. This paper analyzes not only UC D-mMIMO systems consisting exclusively of aerial TRPs carried out by UAVs, but also a setup with mixed of terrestrial and aerial TRPs. The UEs mobility across the coverage area is modeled, and the optimization of the UAVs' trajectories is accomplished by dynamically adjusting the UAVs' positions while the UEs' positions change with time. Additionally, the proposed algorithm uses the DL SE as a metric that links the UAVs' positions with the UEs' performances. This paper also leverages closed-form

expression for MR precoding to compute SE, thus requiring only slow-time varying statistical information and simplifying the optimization process. To the best of the authors' knowledge, this is the first paper which proposes an approach to heuristically optimize the positions and trajectories of aerial TRPs in UC D-mMIMO networks, taking into account the constant UEs' movement in the coverage area. Overall, the main contributions of this paper can be summarized as:

- UC D-mMIMO systems enabled by a swarm of UAVs are analyzed. Specifically, this paper models the DL SE assuming Rician fading, which takes into account the effect of LoS and NLoS propagation. Additionally, the modeling for computational complexity (CC), power consumption, and energy efficiency (EE) in such systems are presented, assuming the relevant parameters related to UAV communication systems.
- A new method for optimizing the trajectory of UAVs has been proposed. This method optimizes the horizontal and vertical locations of each UAV. Additionally, the paper proposes a model for UEs mobility using a discrete-time Markov chain. The proposed trajectory optimization takes into account the constantly changing positions of UEs. By utilizing a time discretization framework, the positioning of UAVs can be adjusted at each time frame, allowing for iterative optimization of the UAVs' trajectories.
- Besides the scenarios consisting exclusive of aerial TRPs carried by UAVs, this paper evaluates hybrid scenarios integrating both aerial and terrestrial TRPs to address challenges associated with high UE density traffic and data rate demands.
- Four precoding strategies are analyzed in terms of SE: MR, local partial MMSE (LP-MMSE), partial regularized zero-forcing (P-RZF), and partial MMSE (P-MMSE). The first two are implemented in a distributed fashion, and the two latter in a centralized fashion. The results show that the proposed algorithm is able to adjust the UAVs' positions with precoding schemes other than MR, even though it is based on simpler MR closed-form expressions for SE.
- The impact of the number of UEs and aerial TRPs on the proposed method's achievable gains is analyzed for different signal processing alternatives. Simulation results reveal that the proposed solution allows for SE improvement of 29.76% for MR, 47.84% for LP-MMSE, 38.14% for P-RZF, and 35.24% for P-MMSE, compared to the case each UAV chooses a random initial position and stay fixed while only UEs move.

C. Paper Outline and Notations

The remainder of this paper is organized as follows. Section II presents the system model, including the channel modeling and estimation procedure, the DL SE, and the CC to perform signal processing. Section III presents the modeling of power consumption and EE. Section IV introduces the proposed approach to optimize the trajectories of UAVs. Section V plots illustrative numerical results and draws insightful discussions to reveal the effectiveness of the proposed approach. Finally, Section VI concludes the paper.

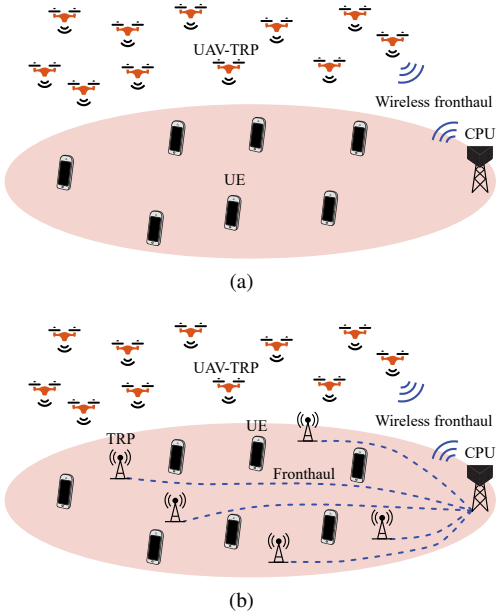

Fig. 1. UC D-mMIMO system enabled by a swarm of UAVs as aerial TRPs. (a) Only aerial TRPs. (b) Terrestrial and aerial TRPs.

Notation: Boldface lowercase and uppercase letters denote column vectors and matrices, respectively, the superscript $(\,.\,)^{\mathrm{H}}$ denotes the conjugate-transpose operation, the $N \times N$ identity matrix is $\mathbf{I}_N$, and the cardinality of the set $\mathcal{A}$ is represented by $|\mathcal{A}|$. The trace, euclidean norm, and expectation operators are denoted as $\mathrm{tr}(\,.\,)$, $\|\,.\,\|$, and $\mathbb{E}\{\,.\,\}$, respectively. The floor, ceiling, and modulus operators are denoted as $\lfloor\,.\,\rfloor$, $\lceil\,.\,\rceil$, and $\%$, respectively. The notation $\mathcal{N}_{\mathbb{C}}\left(\mu, \sigma^2\right)$ stands for a complex Gaussian random variable with mean μ and variance σ^2. $\mathcal{U}[a, b]$ denotes a uniform random variable on the interval $[a, b]$, and $\mathcal{F}(x, \sigma^2, a) \sim \mathcal{TN}(x, \sigma^2, x-a, x+a)$ stands for a truncated normal distribution function in the interval $[x-a, x+a]$ with mean value centered at x degrees and variance σ^2. Moreover, $P\left(X = x | Y = y\right)$ denotes the conditional probability of $X = x$ given $Y = y$, where X and Y are random variables.

II. System Model

We consider a UC D-mMIMO network composed of L TRPs and K single-antenna UEs. Each TRP is equipped with N antennas, and the total number of antennas considering all TRPs is $M = NL$, where $M > K$. The aerial TRPs are deployed at UAVs, and they connect to the CPU through dedicated wireless fronthaul links, as illustrated in Fig. 1a. In the hybrid D-mMIMO system, terrestrial and aerial TRP are deployed, as depicted in Fig. 1b. By denoting the number of terrestrial TRPs as L_t and the number of aerial TRPs as L_a, the total number of TRPs is defined as $L = L_t + L_a$. Additionally, each UE is served by a subset of TRPs. The system operates on time-division duplex (TDD) mode, and it is assumed reciprocity for the UL and DL channels. The channel vector $\mathbf{h}_{kl} \in \mathbb{C}^{N \times 1}$ between the TRP l and UE k undergoes an independent correlated Rician fading, being defined as [21]–[24]

$$\mathbf{h}_{kl} = \underbrace{\sqrt{\frac{\kappa_{kl}\beta_{kl}}{1+\kappa_{kl}}}\mathbf{h}_{kl}^{\mathrm{LoS}}}_{\overline{\mathbf{h}}_{kl}} e^{j\psi_{kl}} + \underbrace{\sqrt{\frac{\beta_{kl}}{1+\kappa_{kl}}}\mathbf{h}_{kl}^{\mathrm{NLoS}}}_{\widetilde{\mathbf{h}}_{kl}}, \quad (1)$$

where $\overline{\mathbf{h}}_{kl} \in \mathbb{C}^{N\times 1}$ corresponds to the deterministic LoS component and $\widetilde{\mathbf{h}}_{kl} \sim \mathcal{N}_{\mathbb{C}}(\mathbf{0}_N, \widetilde{\mathbf{R}}_{kl}) \in \mathbb{C}^{N\times 1}$ is the small-scale fading random component from NLoS propagation with covariance matrix $\widetilde{\mathbf{R}}_{kl} = \mathbb{E}\{\widetilde{\mathbf{h}}_{kl}\widetilde{\mathbf{h}}_{kl}^{\mathrm{H}}\} \in \mathbb{C}^{N\times N}$, κ_{kl} denotes the Rician factor, and β_{kl} is the large-scale fading, including path loss and shadowing. Due to the UEs mobility, random phase shifts $\psi_{kl} \sim \mathcal{U}[0, 2\pi)$ occur in the LoS component, which is assumed to be unknown. Assuming TRPs equipped with a half-wavelength-spacing uniform linear array (ULA), $\mathbf{h}_{kl}^{\mathrm{LoS}} = \left[1, \cdots, e^{-\mathrm{j}(N-1)\pi \sin(\varphi_{kl})\cos(\theta_{kl})}\right]^{\mathrm{T}} \in \mathbb{C}^{N\times 1}$, where φ_{kl} denotes the azimuth angle and θ_{kl} denotes the elevation angle of the LoS component.

The Rician factor κ_{kl} represents the power ratio between the LoS and NLoS components. For LoS propagation links, the Rician factor can be modeled as $\kappa_{kl} = \min\{10^{1.3-0.003 d_{lk}}, p_{\mathrm{LoS}}/(1-p_{\mathrm{LoS}})\}$ [21], [24], where d_{lk} is the between TRP l and UE k, p_{LoS} is the LoS propagation probability. For aerial TRPs, p_{LoS} is a function of the elevation angle θ_{kl}, given by [25]

$$p_{\mathrm{LoS}} = \frac{1}{1 + a\exp\left(-b\left[\frac{180\theta_{kl}}{\pi} - a\right]\right)}, \quad (2)$$

where a and b are determined according to the environment. The large-scale fading β_{kl} is modeled as [25]

$$\beta_{kl}[\mathrm{dB}] = -20\log\left(\frac{4\pi f_c d_{kl}}{c}\right) - \begin{cases} \eta^{\mathrm{LoS}} & \text{for LoS link} \\ \eta^{\mathrm{NLoS}} & \text{for NLoS link} \end{cases}, \quad (3)$$

where the first term denotes the free-space path loss, which is a function of the distance d_{kl} between UE k and TRP l, the carrier frequency f_c, and the speed of light c. The variables η^{LoS} and η^{NLoS} stand for the additional losses that differ according to the environment, and the presence or absence of the LoS component.

A. Uplink Training and Channel Estimation

Each coherence block comprises τ_c samples, where τ_p samples are dedicated for UL pilot signals and τ_d for DL data. In the UL training phase, the UEs send pilot sequences of τ_p-length to the TRPs. Then, the UL channels are estimated using phase-unaware linear minimum mean square error (LMMSE) estimation. The pilot signals are orthogonal to each other, and a pilot t_k can be reused by some UEs if $K > \tau_p$. Let $\mathcal{P}_k \subset \{1, \ldots, K\}$ denote the subset of the UEs assigned to the pilot t_k, including the UE k. The received pilot signal at TRP l can be expressed as [7]

$$\mathbf{y}_{t_k l}^{\mathrm{pilot}} = \sum_{i\in\mathcal{P}_k} \sqrt{\tau_p \eta_i}\, \mathbf{h}_{il} + \mathbf{n}_{t_k l}, \quad (4)$$

where $\mathbf{n}_{t_k l} \sim \mathcal{N}_{\mathbb{C}}\left(\mathbf{0}_N, \sigma_{ul}^2 \mathbf{I}_N\right)$ denotes the noise and η_i is the power that the UE i transmits in the UL direction. The LMMSE channel estimate is given by

$$\widehat{\mathbf{h}}_{kl} = \sqrt{\tau_p \eta_k}\mathbf{R}_{kl}\boldsymbol{\Psi}_{t_k l}^{-1}\mathbf{y}_{t_k l}^{\mathrm{pilot}}, \quad (5)$$

where $\mathbf{R}_{kl} = \mathbb{E}\{\mathbf{h}_{kl}\mathbf{h}_{kl}^{\mathrm{H}}\} = (\overline{\mathbf{h}}_{kl}\overline{\mathbf{h}}_{kl}^{\mathrm{H}} + \widetilde{\mathbf{R}}_{kl})$ and $\boldsymbol{\Psi}_{t_k l} = \mathbb{E}\{(\mathbf{y}_{t_k l}^{\mathrm{pilot}})(\mathbf{y}_{t_k l}^{\mathrm{pilot}})^{\mathrm{H}}\} = \sum_{i\in\mathcal{P}_k} \eta_i \tau_p (\overline{\mathbf{h}}_{il}\overline{\mathbf{h}}_{il}^{\mathrm{H}} + \widetilde{\mathbf{R}}_{il}) + \sigma_{\mathrm{ul}}^2 \mathbf{I}_N$.

B. Downlink Data Transmission

In UC systems, each UE is associated with a subset of TRPs called TRP cluster, represented by $\mathcal{M}_k \subset \{1, \ldots, L\}$. The connections between the UE k and TRPs are denoted by a diagonal matrix $\mathbf{D}_{kl} \in \mathbb{N}^{N\times N}$, being defined as

$$\mathbf{D}_{kl} = \begin{cases} \mathbf{I}_N & \text{if } l \in \mathcal{M}_k \\ \mathbf{0}_N & \text{if } l \notin \mathcal{M}_k. \end{cases} \quad (6)$$

The subset of UEs served by a TRP is denoted by $\mathcal{D}_l \subset \{1, \ldots, K\}$. In this work, the number of UEs that each TRP can serve ($K_l = |\mathcal{D}_l|$) and the number of TRPs connected to each UE ($L_k = |\mathcal{M}_k|$) are limited, such that $K_l \leq \tau_p$ and $L_k \leq C_{\max}$. This is performed in order to comply with the scalability requirements and to reduce the processing complexity from the network [5], [26], [27]. Let $s_k \in \mathbb{C}$ denote the symbol intended for the UE k. The DL received signal at the UE k can be given by

$$y_k^{\mathrm{dl}} = \sum_{l=1}^{L} \underbrace{\mathbf{h}_{kl}^{\mathrm{H}}\mathbf{D}_{kl}\mathbf{w}_{kl}s_k}_{\text{Desired signal}} + \sum_{i=1, i\neq k}^{K}\sum_{l=1}^{L} \underbrace{\mathbf{h}_{kl}^{\mathrm{H}}\mathbf{D}_{il}\mathbf{w}_{il}s_i}_{\text{Interfering signals}} + \underbrace{n_k}_{\text{Noise}}, \quad (7)$$

where $\mathbf{x}_l = \sum_{k=1}^{K} \mathbf{D}_{kl}\mathbf{w}_{kl}s_k$ represents the data signal sent by the TRP l, $\mathbf{w}_{kl}$ denotes the precoding vector, and $n_k \sim \mathcal{N}_{\mathbb{C}}\left(0, \sigma_{\mathrm{dl}}^2\right)$ is the receiver noise. The terms s_k and $\mathbf{w}_{kl}$ satisfy $\mathbb{E}\left\{\|s_k\|^2\right\} = 1$ and $\mathbb{E}\left\{\|\mathbf{w}_{kl}\|^2\right\} = \rho_{kl}$, with ρ_{kl} being the power allocated to the UE k regarding the TRP l. The DL power of each TRP is restricted to ρ_l, such that $\sum_{k\in\mathcal{D}_l}\rho_{kl} \leq \rho_l$. From (7), an achievable DL SE can be computed as [5]

$$\mathrm{SE}_k = \frac{\tau_d}{\tau_c}\log_2\left(1 + \mathrm{SINR}_k\right), \quad (8)$$

where SINR_k denotes the DL SINR, which is given by

$$\mathrm{SINR}_k = \frac{\left|\mathbb{E}\left\{\mathbf{h}_k^{\mathrm{H}}\mathbf{D}_k\mathbf{w}_k\right\}\right|^2}{\sum_{i=1}^{K}\mathbb{E}\left\{\left|\mathbf{h}_k^{\mathrm{H}}\mathbf{D}_i\mathbf{w}_i\right|^2\right\} - \left|\mathbb{E}\left\{\mathbf{h}_k^{\mathrm{H}}\mathbf{D}_k\mathbf{w}_k\right\}\right|^2 + \sigma_{\mathrm{dl}}^2}, \quad (9)$$

where $\mathbf{w}_k \in \mathbb{C}^{M\times 1}$ and $\mathbf{h}_k \in \mathbb{C}^{M\times 1}$ are, respectively, the collective vectors of $\mathbf{w}_{kl}$ and $\mathbf{h}_{kl}$. For instance, $\mathbf{w}_k = \left[\mathbf{w}_{k1}^{\mathrm{T}}, ..., \mathbf{w}_{kL}^{\mathrm{T}}\right]^{\mathrm{T}}$ for $l \in \{1, \cdots, L\}$. Moreover, $\mathbf{D}_k = \mathrm{diag}\left(\mathbf{D}_{k1}, ..., \mathbf{D}_{kL}\right) \in \mathbb{N}^{M\times M}$ stands for the diagonal block matrix. In (9), all expectations are related to the channel small-scale fading realizations [7]. Note that (8) and (9) represent the widely known hardening bound, which is a capacity lower bound valid for any choice of precoding vectors [5]. Unfortunately, the SINR does not have a closed-form expression when using P-MMSE, P-RZF, and LP-MMSE precoding schemes. However, it is still possible to compute the SINR through Monte-Carlo simulations.

C. Signal Processing Computational Complexity

In the centralized implementation, the CPUs perform channel estimation and combining/precoding computation [5]. In the distributed one, the TRPs perform these tasks locally, and

the CPUs encode the DL data signals. The CC for combining and precoding-related operations is calculated as in [7], [28], accounting for the sum of the number of complex operations (multiplications and divisions) required in each coherence block.

For distributed MR precoding, the number of complex operations for each TRP l is given

$$C_l^{\mathrm{MR}} = \left(N\tau_p + N^2\right)|\mathcal{D}_l|, \tag{10}$$

which represents only LMMSE channel estimation procedure. For distributed LP-MMSE, it becomes

$$\begin{aligned} C_l^{\mathrm{LP-MMSE}} = \left(N\tau_p + N^2\right)|\mathcal{D}_l| + \frac{1}{2}(N^2+N)|\mathcal{D}_l| \\ + N^2|\mathcal{D}_l| + \frac{1}{3}(N^3 - N) + N, \end{aligned} \tag{11}$$

which accounts for LMMSE channel estimation, matrix inversion and product. It can be noticed that the CC is a function of the number of UEs served by each TRP ($|\mathcal{D}_l|$) in the distributed implementation.

In the centralized precoding schemes, the number of complex operations depends on the number of TRPs serving each UE ($|\mathcal{M}_k|$) and the number of UEs that are served by partially the same TRPs as the UE k, denoted as $\mathcal{S}_k = \{i : \mathbf{D}_k\mathbf{D}_i \neq \mathbf{0}_{LN\times LN}\}$. For P-MMSE precoding, there are tasks of different TRPs performed only once for each UE. The common TRPs that serve UE k and $i \in \mathcal{S}_k$ is denoted by the set $\mathcal{B}_k = \cup_{i\in\mathcal{S}_k}\mathcal{M}_i$. Then, the total number of complex operations is given by

$$\begin{aligned} C^{\mathrm{P-MMSE}} = \sum_{k=1}^{K}\Bigg\{ \left(N\tau_p + N^2\right)|\mathcal{B}_k| + \frac{1}{2}\left((N|\mathcal{B}_k|)^2 + N|\mathcal{B}_k|\right) \\ + (N|\mathcal{M}_k|)^2 + \frac{1}{3}\left((N|\mathcal{M}_k|)^3 - N|\mathcal{M}_k|\right) + N|\mathcal{M}_k| \Bigg\}. \end{aligned} \tag{12}$$

For P-RZF, the total number of complex operations is given by

$$\begin{aligned} C^{\mathrm{P-RZF}} = \sum_{l=1}^{L}\left\{ \left(N\tau_p + N^2\right)|\mathcal{C}_l| + \frac{1}{2}\left(|\mathcal{C}_l|^2 + |\mathcal{C}_l|\right)N \right\} \\ + \sum_{k=1}^{K}\left\{ |\mathcal{S}_k|^2 + N|\mathcal{M}_k||\mathcal{S}_k| + \frac{1}{3}\left(|\mathcal{S}_k|^3 - |\mathcal{S}_k|\right) + |\mathcal{S}_k| \right\}, \end{aligned} \tag{13}$$

where $\mathcal{C}_l = \cup_{l'\in\mathcal{M}_{k\in\mathcal{D}_l}}\mathcal{D}_{l'}$ denotes the set of common UEs that are served by TRP l and $l' \in \mathcal{M}_{k\in\mathcal{D}_l}$. The subset $\mathcal{C}_l$ is defined since there are common tasks regarding different UEs that are performed only once for each TRP l, such as the LMMSE channel estimation.

In terms of hardware computational complexity, the number of complex operations can be converted to giga operations per second (GOPS) required by the TRPs and CPU. This leads to the multiplicative factor $f = 8N_{\mathrm{DFT}}(\tau_c T_s)^{-1}\times 10^{-9}$ for conversion from the number of complex operations to GOPS. The number of GOPS required by the TRPs is given by [29]

$$\mathrm{GOPS}_l = If\left\{C_l^{\mathrm{est/comb}} + C_l^{\mathrm{cal/prec}}\right\} + C_l^{\mathrm{DFT}} + C_l^{\mathrm{BBF}}, \tag{14}$$

where $I \in \{0,1\}$ is a binary variable that indicates if centralized ($I=0$) or distributed ($I=1$) processing is used. In the first term, $C_l^{\mathrm{est/comb}} \in \{C_l^{\mathrm{MR}}, C_l^{\mathrm{LP-MMSE}}\}$ since only distributed processing is performed in the TRPs, and $C_l^{\mathrm{cal/prec}} = N|\mathcal{D}_l|(1+\tau_d)$ represents the number of complex multiplications required to perform reciprocity calibration and precoding application. The terms $C_l^{\mathrm{DFT}} = 8NN_{\mathrm{DFT}}\log_2(N_{\mathrm{DFT}})/T_s 10^9$ and $C_l^{\mathrm{BBF}} = 40Nf_s/10^9$ are the required GOPS for the discrete Fourier transform (DFT) and the baseband filter [30], [31], respectively.

The required GOPS for the CPU is given by [29]

$$\mathrm{GOPS}_{\mathrm{CPU}} = (1-I)f\left\{C^{\mathrm{est/comb}} + C^{\mathrm{cal/prec}}\right\} + C_{\mathrm{CPU}}^{\mathrm{other}}, \tag{15}$$

where $C^{\mathrm{est/comb}} \in \{C^{\mathrm{P-MMSE}}, C^{\mathrm{P-RZF}}\}$ since only centralized precoding are performed at the CPU, $C^{\mathrm{cal/prec}} = \sum_{l=1}^{L} N|\mathcal{D}_l|(1+\tau_d)$ accounts for reciprocity calibration and precoding application, and $C_{\mathrm{CPU}}^{\mathrm{other}}$ denotes the CC in GOPS the CPU demands to perform other operations that are common for centralized and distributed processing, given by [32]

$$\begin{aligned} C_{\mathrm{CPU}}^{\mathrm{other}} = &(B/B_{\mathrm{b}})^1\left(\overline{\mathrm{SE}}/\mathrm{SE}_{\mathrm{b}}\right)^1 C_{\mathrm{HLN}} + (LN)^{0.5}K^{0.2}C_{\mathrm{HLC}} \\ &+ (B/B_{\mathrm{b}})^1\left(\overline{\mathrm{SE}}/\mathrm{SE}_{\mathrm{b}}\right)^1 K^1 C_{\mathrm{ChC}} \\ &+ (B/B_{\mathrm{b}})^1\left(\overline{\mathrm{SE}}/\mathrm{SE}_{\mathrm{b}}\right)^{1.5} K^1 C_{\mathrm{MD}} + (B/B_{\mathrm{b}})^1 K^1 C_{\mathrm{OFDM}}, \end{aligned} \tag{16}$$

where C_{HLN}, C_{HLC}, C_{ChC}, C_{MD}, C_{OFDM} are the base GOPS for higher-layer network (HLN), higher-layer control (HLC), channel coding, layer mapping and demapping, and orthogonal frequency-division multiplexing (OFDM) modulation and demodulation, respectively.

III. Power Consumption and Energy Efficiency Modeling

The total power consumption can be formulated as

$$P_{\mathrm{tot}} = \sum_{l=1}^{L}\left\{P_l + P_{\mathrm{fh},l} + A_l P_{\mathrm{UAV},l}\right\} + P_{\mathrm{CPU}}, \tag{17}$$

where P_l is the power consumed by each TRP for data transmission, $P_{\mathrm{fh},l}$ is the power that the fronthaul link connecting the CPU and TRP l consumes, and P_{CPU} is the power required by the CPU to perform the signal processing tasks. Additionally, $P_{\mathrm{UAV},l}$ represents the power required for a UAV to fly to a location and hover at a fixed point, and $A_l \in \{0,1\}$ is a binary variable that indicates if the TRP l is terrestrial ($A_l = 0$) or aerial ($A_l = 1$).

The total EE in bit/Joule, is computed as the ratio between the sum throughput in bit/s and the total power consumed in Watts (W) [33], [34]. It can be written as

$$\mathrm{EE}_{\mathrm{tot}} = \frac{B\sum_{k=1}^{K}\mathrm{SE}_k}{P_{\mathrm{tot}}}, \tag{18}$$

where B is the bandwidth.

A. Power Consumption of each TRP

The power consumed by each UAV, including data transmission, effects of amplifier and circuit of the analog front-end, is modeled as

$$P_l = \frac{1}{\gamma_l}\mathbb{E}\left\{\|\mathbf{x}_l\|^2\right\} + NP_{\mathrm{tc},l} + P_{\mathrm{CC},l}, \tag{19}$$

where $0 < \gamma_l \leq 1$ denotes the efficiency of the power amplifier, and $P_{\mathrm{tc},l}$ is the power required of each antenna

of the TRP l to run internal components, such as converters and filters, $P_{\mathrm{CC},l}$ is the power required to perform the signal processing tasks at the TRPs, given by

$$P_{\mathrm{CC},l} = P_{l,0}^{\mathrm{proc}} + \Delta_{l}^{\mathrm{proc}} \left(\frac{CC_l}{CC_l^{\max}} \right), \tag{20}$$

where $P_{l,0}^{\mathrm{proc}}$ denotes the power consumed by each digital signal processor (DSP) of TRP l in idle mode, $\Delta_{\mathrm{RU},l}^{\mathrm{proc}}$ represents the slope of power consumption due to processing, and $CC_l^{\max}$ indicates the maximum GOPS capacity of the DSP.

B. UAV Propulsion Power Consumption

It is assumed that each UAV flies to the target deployment point, hovers during the service time, and returns to the initial point. Depending on the type of flight, the propulsion power of the UAV is $P_{\mathrm{UAV},l} = P_{\mathrm{hv},l}$ if it hovers or $P_{\mathrm{UAV},l} = P_{\mathrm{cv},l}$ if the UAV is flying.

The power required for a UAV to hover is given by [35]

$$P_{\mathrm{hv},l} = \frac{(m_{\mathrm{tot}} g)^{3/2}}{\eta \sqrt{2 r \rho \varsigma}}, \tag{21}$$

where m_{tot} is the total mass of each UAV, including the battery and TRP components, g is the gravity acceleration, ρ is the air density, η denotes the battery and motor power transfer efficiency. Moreover, r represents the number of rotors for a rotocopter drone, and ς stands for the area of the spinning blade disc of one rotor.

The power required for the UAV l to fly at a constant air velocity v_l in m/s is given by [36]

$$P_{\mathrm{cv},l} = \frac{T \left(v_l \sin \alpha + v_{\mathrm{ind},l} \right)}{\eta}, \tag{22}$$

where $T = W + D = m_{\mathrm{tot}} g + \frac{1}{2} \rho C_D A v_l^2$, and $\alpha = \tan^{-1}\left(\frac{D}{W}\right)$. C_D and A are the drone's drag coefficient and projected area, respectively. The induced velocity $v_{\mathrm{ind},l}$ can be numerically computed by

$$v_{\mathrm{ind},l} = \frac{m_{\mathrm{tot}} g}{2 r \rho \varsigma \sqrt{\left(v_l \cos \alpha \right)^2 + \left(v_l \sin \alpha + v_{\mathrm{ind},l} \right)^2}}. \tag{23}$$

C. Fronthaul Traffic Rate and Power Consumption

The rate in the fronthaul links is also different depending on the type of network implementation, i.e., centralized and distributed processing. For distributed processing, the rate scales with the number of UEs served by the TRP, while in the centralized implementation, it scales with the number of antennas in the TRP. The fronthaul traffic is modeled as [37]

$$R_{\mathrm{fh},l} = 2B \left(I \frac{\tau_d}{\tau_c} \sum_{k \in \mathcal{D}_l} b_{kl}^d + (1 - I) N \left(b_l^d \frac{\tau_d}{\tau_c} + b_l^p \frac{\tau_p}{\tau_c} \right) \right), \tag{24}$$

where b_{kl}^d is the number of quantization bits per sample of each UE used for data transmissions in the distributed implementation, and b_l^d and b_l^p are the quantization bits per sample used for data and pilot signals in each TRP, respectively, in the centralized implementation.

The power that the fronthaul link consumes is modeled as

$$P_{\mathrm{fh},l} = P_{0,l} + P_{\mathrm{ft},l} R_{\mathrm{fh},l}, \tag{25}$$

where $P_{0,l}$ is a fixed power consumption of each fronthaul (traffic-independent power), which may depend on the distances between the TRPs and the CPU and the system topology, $P_{\mathrm{ft},l}$ is the traffic-dependent power (in Watt per bit/s), and $R_{\mathrm{fh},l}$ the rate in each fronthaul link, that is different depending on the type of network implementation, i.e., centralized and distributed processing.

D. CPU Power Consumption

The power consumed by the CPU can be expressed as

$$P_{\mathrm{CPU}} = P_{\mathrm{fixed}} + \frac{1}{\sigma_{\mathrm{cool}}} \left(N_{\mathrm{GPP}} P_{\mathrm{GPP},0}^{\mathrm{proc}} + \Delta_{\mathrm{GPP}}^{\mathrm{proc}} \frac{CC_{\mathrm{CPU}}}{CC_{\mathrm{GPP}}^{\max}} \right), \tag{26}$$

where P_{fixed} represents the fixed power consumption of each CPU, $0 < \sigma_{\mathrm{cool}} \leq 1$ denotes the cooling efficiency, $N_{\mathrm{GPP}} = \lceil CC_{\mathrm{CPU}} / CC_{\mathrm{GPP}}^{\max} \rceil$ is the number of active general purpose processors (GPPs), $P_{\mathrm{GPP},0}^{\mathrm{proc}}$ is the idle power consumption, $\Delta_{\mathrm{GPP}}^{\mathrm{proc}}$ stands for the slope of power consumption, and $CC_{\mathrm{GPP}}^{\max}$ is the maximum processing capacity in GOPS.

IV. UAV Trajectory Optimization

This section introduces the algorithms to model the UEs mobility and to optimize the trajectory of the UAVs. Recall that in the context of UC D-mMIMO networks, UAVs act as mobile TRPs, and thus, their positioning in the coverage area is intrinsically associated with the system performance. Therefore, the decision process to update the positions of UAVs can be based on network performance metrics, such as SE and EE, as computed in (8) and (18). However, such metrics can change frequently in wireless channels due to channel fading and UEs mobility.

An alternative solution involves using a discretization framework, where the positioning of UAVs can be adjusted in each time frame, in conjunction with the large-scale fading coefficients, which remain unchanged for many coherency blocks. This consideration allows the calculation of a tractable ergodic UEs SE metric using only large-scale channel state information (CSI). The SE is calculated on a given disposition of UEs and TRPs in each time frame. For the MR precoding, the closed-form expressions for SE can be computed as [38]

$$\mathbb{E}\left\{ \mathbf{h}_k^{\mathrm{H}} \mathbf{D}_k \mathbf{w}_k \right\} = \sum_{l \in \mathcal{M}_k} \sqrt{\rho_{kl} \eta_k \tau_p \mathrm{tr}(\mathbf{R}_{kl} \boldsymbol{\Psi}_{t_k l}^{-1} \mathbf{R}_{kl})}, \tag{27}$$

$$\begin{aligned} \mathbb{E}\left\{ \left| \mathbf{h}_k^{\mathrm{H}} \mathbf{D}_i \mathbf{w}_i \right|^2 \right\} = & \sum_{l \in \mathcal{M}_i} \widehat{\rho}_{il} \eta_i \tau_p \mathrm{tr}\left(\mathbf{R}_{kl} \boldsymbol{\Omega}_{il} \right) + \\ & P_{ik} \left\{ \sum_{l \in \mathcal{M}_i} \widehat{\rho}_{il} \eta_i \eta_k \tau_p^2 \left[\mathrm{tr}\left(\widetilde{\mathbf{R}}_{kl}^2 \boldsymbol{\Psi}_{t_i l}^{-1} \boldsymbol{\Omega}_{il} \right) \right. \right. \\ & \left. + 2\mathrm{tr}\left(\boldsymbol{\Omega}_{il} \boldsymbol{\Psi}_{t_i l}^{-1} \mathbf{L}_{kl} \widetilde{\mathbf{R}}_{kl} \right) - \mathrm{tr}\left(\left(\mathbf{R}_{kl} \boldsymbol{\Psi}_{t_i l}^{-1} \mathbf{R}_{il} \right)^2 \right) \right] \\ & \left. + \left| \sum_{l \in \mathcal{M}_i} \sqrt{\widehat{\rho}_{il} \eta_i \eta_k \tau_p^2} \mathrm{tr}\left(\mathbf{R}_{kl} \boldsymbol{\Psi}_{t_i l}^{-1} \mathbf{R}_{il} \right) \right|^2 \right\}, \end{aligned} \tag{28}$$

where $\mathbf{\Omega}_{il} = \mathbf{R}_{il}\mathbf{\Psi}_{t_i l}^{-1}\mathbf{R}_{il}$, $\widehat{\rho}_{il} = \rho_{il}/\mathrm{tr}(\eta_i \tau_p \mathbf{\Omega}_{il})$, $\mathbf{L}_k = \overline{\mathbf{h}}_{kl}\overline{\mathbf{h}}_{kl}^{\mathrm{H}}$, and $P_{ik} \in \{0,1\}$ is a binary variable that indicates if different UEs share the same pilot sequence, that is, $P_{ik} = 1$ if $i \in \mathcal{P}_k$, and $P_{ik} = 0$ if $i \notin \mathcal{P}_k$. Moreover, (27) represents the desired signal power, and (28) is the interference signals power. One can observe that using more complex precoding schemes with superior interference cancellation capabilities, such as P-MMSE and LP-MMSE, do not allow for SE computation based on large-scale gains, as there are no closed-form equations available for non-MR linear precoding. Despite this limitation, the network can be optimized to MR while operating with any type of precoding. Although this strategy does not yield globally optimized performance, it balances optimization complexity and overall system performance.

The flowchart depicted in Fig. 2 provides an overview of the approach employed in this paper to update the UAVs' positioning. Initially, all UAVs are placed in arbitrary positions, e.g., random or evenly spaced, and then ergodic metrics based on long-term statistics are evaluated. If a target SE is not achieved, the new candidate UAVs' positions are calculated based on long-term metrics, the positions that leads to the highest performance metric are selected, as detailed in Subsection IV-B. Then, the coordinated trajectories of UAVs are computed in order to avoid collisions when UAVs move. The UAVs' positions will be updated until a target SE is achieved, otherwise, their positions will be fixed.

In this paper, $\mathrm{n_s}$ setups account for different UEs and UAVs initial positions. Over $\mathrm{n_e}$ episodes, UEs' positions change according to their mobility behaviors, while the UAVs' positions may either remain static or be dynamically optimized by the proposed algorithm. If optimization occurs, each episode is subdivided into $\mathrm{n_i}$ iterations. During these iterations, UAVs may adjust their positions in search of the optimal location iteratively, whereas UEs maintain their positions. At the end of all iterations inside an episode, UAVs assume positions where maximum SE performance was obtained to have the best next episode initial position. This process is then replicated across all setups to compile the statistical numerical results of this paper. The following subsections detail the proposed models for UEs mobility and UAVs position adjustment, respectively.

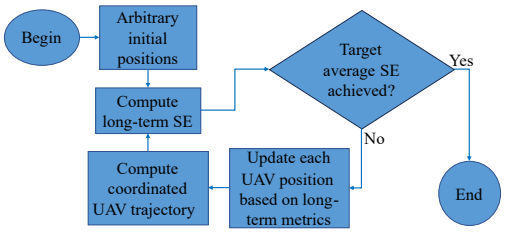

Fig. 2. Flowchart outlining the process for determining whether or not to update the positions of UAVs.

A. UEs Mobility Modeling

It is considered that UEs are deployed randomly in the streets of an urban scenario with multiple buildings. The UEs may move in different directions as long they remain inside the coverage area and streets. For simplification, it is assumed that each UE can move at angles, given in degrees, denoted by $\phi_k \in \mathcal{A}_\phi$, where $\mathcal{A}_\phi = \{\phi^{\min}, \phi^{\min} + \phi^{\mathrm{step}}, ..., \phi^{\max}\} = \{a_1, a_2+, \cdots, a_{|\mathcal{A}_\phi|}\}$. Moreover, it is important to note that $\phi^{\min} \geq 0$ is the minimum direction angle, $0 \leq \phi^{\mathrm{step}} \leq 360$ is the step between considered angles, and $\phi^{\max} \leq 360$ is the maximum direction angle.

A discrete-time Markov chain with $|\mathcal{A}_\phi| + 1$ states is used to model the mobility of each UE, as shown in Fig. 3. The additional state concerning the number of possible movement directions exists to model stationary positioning behavior. Under this model, it is established a probability transition matrix $\mathbf{P} = [p_{i,j}]$, with $i \in \{1, \cdots, |\mathcal{A}_\phi| + 1\}$ and $j \in \{1, \cdots, |\mathcal{A}_\phi| + 1\}$. In this context, $p_{1,1}$ is the probability of a stationary UE to continue in this condition, which is given by p_{s}. Conversely, $p_{1,i}$ for all $i \in \{2, \cdots, |\phi_k| + 1\}$ represents the probability of a UE initiating movement in any direction, being calculated as $(1 - p_s)/|\mathcal{A}_\phi|$, implying an equal probability of moving in any direction. Furthermore, $p_{i,1}$ for all $i \in \{2, \cdots, |\mathcal{A}_\phi| + 1\}$, indicates the probability of a moving UE coming to a halt, which is given by p_h.

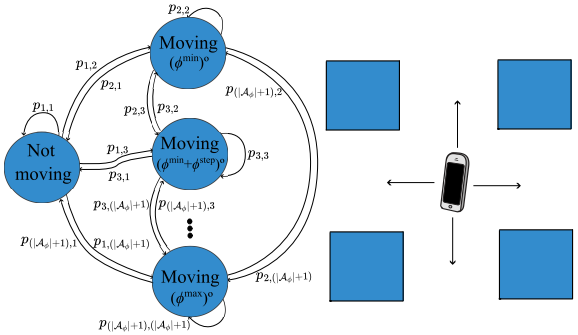

Fig. 3. UEs moving directions modeled by a discrete-time Markov chain, where the UEs moving directions depend on their previous direction of movement. The UEs positions are a function of their speeds, current moving directions, and previous positions.

The probabilities $p_{i,j}$ for $i \neq 1$ and $j \neq 1$ are hard to calculate. UEs in motion are expected to have specific destinations, leading to a generally consistent direction of movement with only minor angle adjustments, except for sudden and more significant changes at locations, like intersections or possible backtracking. These considerations imply that the probability of UEs maintaining a similar direction of movement is very high, while the likelihood of adopting an opposite direction is very low. To model this behavior, the movement direction of a UE in episode n, where $n > 1$, if it does not come to a halt, is given by a random variable $\phi_k^{(n)} \sim \mathcal{F}(\phi_k^{(n-1)}, \sigma_\phi, 180)\%360$, where $\%$ stands for the modulus operator, $\mathcal{F}(x, \sigma^2, 180) \sim \mathcal{TN}(x, \sigma^2, x - 180, x + 180)$ stands for a truncated normal distribution function, σ_ϕ is a variance that models the UEs commitment to maintain a similar direction of movement. Under this distribution, the probability $p_{i,j}$ for $i \neq 1$ and $j \neq 1$ is given by

$$p_{i,j} = (1 - p_h) P\left(\phi_k^{(n)} = a_j | \phi_k^{(n-1)} = a_i\right). \quad (29)$$

Finally, the UEs positions in the two-dimensional Cartesian

space in episode n are modeled as

$$\begin{aligned} x_k^{(n)} &= v_k^{(n)} \Delta_n \cos\left(\pi \phi_k^{(n)}/180\right) + x_k^{(n-1)} \\ y_k^{(n)} &= v_k^{(n)} \Delta_n \sin\left(\pi \phi_k^{(n)}/180\right) + y_k^{(n-1)} \end{aligned}, \tag{30}$$

where Δ_n is the time step between episodes. It is worth noting that the boundaries of the buildings and coverage area serve as obstacles. Hence, whenever a UE approaches them, it can only move away in the opposite direction. Moreover, in each episode, the UEs move at different speeds up to a maximum value $v_{\max}$, which is randomly defined as $v_k^{(n)} \sim \mathcal{U}[0, v_{\max}]$ for each UE k.

B. 3D Trajectory of UAVs

This subsection presents the steps to adjust the UAVs' positions. An iterative method is designed with the goal of improving UEs' SE performance. The algorithm works by defining the total number of iterations it has available to operate while the UEs are assumed to be in a stationary position. For that purpose, the number of iterations is defined as the ratio between the UAVs and UEs maximum velocities, i.e., $\mathrm{n_i} = \max_{l\in\{1,\dots,L\}}(v_l)/\max_{k\in\{1,\dots,K\}}(v_k)$, where v_l and v_k are the velocities of UAV l and UE k, respectively. The impact of UAVs positions on the UEs' performance can be computed based on long-term CSI. Specifically, for any combination of UEs and UAVs locations, the SE of the UEs can be obtained replacing (27) and (28) in (9) and (8). Although these equations are specific for MR precoding, they are still useful to provide a good estimate of the UEs' performance even if another precoding technique is later performed.

The first step of the algorithm is to define a set of UAVs chosen to update their positions in the current episode. This is performed based on the average SE obtained at the start of a new episode. Specifically, the set $\mathcal{M}_{k^{\min}} \subset \{1,\dots,L\}$ defines the UAVs that serve the UE with the worst SE performance, where $k^{\min} = \arg\min_k \mathrm{SE}_k$. It is important to note that only a subset of UAVs update their positions in each episode due to the limited number of iterations ($\mathrm{n_i}$) available.

In the next step of the algorithm, the total number of iterations is divided by the number of UAVs in the set ($\mathrm{n_i}^{\mathrm{UAV}} = \mathrm{n_i}/|\mathcal{M}_{k^{\min}}|$). The goal of this step is that each UAV adjusts its position individually, guaranteeing the SE is not affected by the movements of other UAVs. At each iteration, the UAV defines its moving direction $\delta_l^{(i)} = \{0, \delta^{\mathrm{step}}, ..., 360\}$ (in degrees), the UAV l position in the two-dimensional Cartesian space is modeled as

$$\begin{aligned} x_l^{(i)} &= v_l \Delta_i \cos\left(\pi \delta_l^{(i)}/180\right) + x_l^{(i-1)} \\ y_l^{(i)} &= v_l \Delta_i \sin\left(\pi \delta_l^{(i)}/180\right) + y_l^{(i-1)} \end{aligned}, \tag{31}$$

where Δ_i is the time step between iteration.

The UAVs included in the set $\mathcal{M}_{k^{\min}}$ take turns adjusting their positions one at a time, where each one has $\mathrm{n_i}^{\mathrm{UAV}}$ iterations available. The selected UAV begins by moving in a random direction, drawn from a uniform discrete distribution $\mathcal{U}[0, 360]$. Subsequently, it computes the SE improvement or reduction related to this movement, computed as

$$\mathrm{SE}_{\mathrm{diff}}^{(i)} = \frac{1}{K}\sum_{k=1}^{K}\left(\mathrm{SE}_k^{(i)} - \mathrm{SE}_k^{(i-1)}\right). \tag{32}$$

In the next iteration, the movement direction of the UAV is determined based on the result of the previous action. If the previous direction led to an increase in SE, the UAV is likely to move in a similar direction. Conversely, if the previous direction resulted in a decrease in SE, the UAV is more likely to move in the opposite direction. In both cases, the next direction is chosen randomly from a normal distribution with a mean equal to the previous direction (or its opposite) and a variance calculated based on the SE improvement (or decrease) of the previous action. However, if there is no SE improvement or decrease, the UAV moves in a uniformly random direction. Therefore, the UAV l movement direction at iteration i is modeled as

$$\delta_l^{(i)} \sim \begin{cases} \mathcal{U}[0, 360] & \text{if } \mathrm{SE}_{\mathrm{diff}}^{(i-1)} = 0 \text{ or } i = 1, \\ \left[\mathcal{F}(\delta_l^{(i-1)}, \sigma_\delta^{(i-1)}, 180)\right] \,\%\, 360 & \text{if } \mathrm{SE}_{\mathrm{diff}}^{(i-1)} > 0, \\ \left[\mathcal{F}(\bar{\delta}_l^{(i-1)}, \sigma_\delta^{(i-1)}, 180)\right] \,\%\, 360 & \text{if } \mathrm{SE}_{\mathrm{diff}}^{(i-1)} < 0, \end{cases} \tag{33}$$

where $\%$ stands for the modulus operator, $\bar{\delta}_l^{(i-1)} = (180 + \delta_l^{(i-1)}) \,\%\, 360$ is the opposite angle of $\delta_l^{(i-1)}$, $\mathcal{F}(x, \sigma^2, 180) \sim \mathcal{TN}(x, \sigma^2, x - 180, x + 180)$ stands for a truncated normal distribution function with mean value centered at x degrees and variance σ^2. The variance parameter is computed based on the SE improvement (or reduction) as

$$\sigma_\delta^{(i-1)} = \min\left(\sigma_\delta^{\max}, \frac{1}{\left|\mathrm{SE}_{\mathrm{diff}}^{(i-1)}\right|}\right), \tag{34}$$

where $\sigma_\delta^{\max}$ is a project parameter. At the end of the iterations, UAV l adjusts its position to the iteration that led to the highest SE performance, i.e., $i^\star = \arg\max_i \sum_{k=1}^{K} \mathrm{SE}_k^{(i)}$. The algorithm concludes once all UAVs adjust their positions. Algorithm 1 summarizes the heuristic method proposed to adjust the UAVs positions.

Furthermore, UAVs heights $z_l^{(i)}$ can also be dynamically optimized in each iteration, where $z_{\min} \le z_l^{(i)} \le z_{\max}$. In this case, a fraction of the iterations allocated for each selected UAV is used to adjust its height while its two-dimensional position remains the same, i.e., $[x_l^{(i)} = x_l^{(i-1)}, y_l^{(i)} = y_l^{(i-1)}]$. For that purpose, a modified version of Algorithm 1 is used, considering that each UAV moves upwards or downwards in a given iteration, represented as $z_{l,(\mathrm{u/d})}^{(i)} \in \{-1, 1\}$. Additionally, the UAV l height is modeled as $z_l^{(i)} = v_l \, \Delta_i \, z_{l,(\mathrm{u/d})}^{(i)} + z_l^{(i-1)}$. Afterward, if the previous action resulted in a SE increase, it continues to move in that direction. Otherwise, it goes in the opposite direction. The process may stop before the end of the assigned iterations if the UAV reaches the minimum or maximum heights.

Note that only channel statistics are needed to compute the proposed UAV trajectory optimization in Algorithm 1, and that it considers imperfect CSI to calculate the UEs' SE. Analyzing the proposed algorithm, the time complexity can be written as $\mathcal{O}(\mathrm{n_i} K^2 |\mathcal{M}_i| N^3)$, which is due to the computation of the UEs' SE for each iteration. For scalability purposes, this work assumes that $|\mathcal{M}_i| \le C_{\max}$, and that the CPU can compute the SE of only $K \le K_{\max} = L C_{\max}$ UEs,

Algorithm 1: Iterative adjustment method for the positions of selected UAVs per episode.

Input: Current episode n, number of iterations $\mathrm{n_i}$, maximum variance parameter $\sigma_\delta^{\max}$, $\mathrm{SE}_{\mathrm{diff}}^{(1)} = 0$.

// Compute the SE at start of episode n

Compute $\mathrm{SE}_k^{(i=0)} = \mathrm{SE}_k^{(n)}\ \forall k \in \{1, \dots K\}$ by solving (27) and (28) in (9) and (8);

// Select the UAVs that serve the worst UE

Set $k^{\min} = \arg\min_k \mathrm{SE}_k^{(n)}$;

Set $\mathcal{M}_{k^{\min}} \subset \{1, \dots, L\}$ as the subset of UAVs that serve the UE with the worst SE performance;

// Define the number of iteration per UAV

Set $\mathrm{n_i}^{\mathrm{UAV}} = \mathrm{n_i}/|\mathcal{M}_{k^{\min}}|$;

// Update the position iteratively

for $l = 1$ **to** $|\mathcal{M}_{k^{\min}}|$ **do**

  for $i = 1$ **to** $\mathrm{n_i}^{\mathrm{UAV}}$ **do**

    if $i = 1$ **or** $\mathrm{SE}_{\mathrm{diff}}^{(\mathrm{i})} = 0$ **then**

      // Move in a random direction

      Set $\delta_l^{(i)} \sim \mathcal{U}[0, 360]$;

    end

    else if $\mathrm{SE}_{\mathrm{diff}}^{(\mathrm{i})} < 0$ **then**

      // Higher probability of moving in the opposite direction

      Set opposite angle as $\bar{\delta}_l^{(i-1)} = (180 + \delta_l^{(i-1)})\,\%\,360$;

      Set $\delta_l^{(i)} \sim \left[\mathcal{F}(\bar{\delta}_l^{(i-1)}, \sigma_\delta^{(i-1)}, 180)\right]\,\%\,360$;

    end

    else

      // Higher probability of moving in similar direction

      Set $\delta_l^{(i)} \sim \left[\mathcal{F}(\delta_l^{(i-1)}, \sigma_\delta^{(i-1)}, 180)\right]\,\%\,360$;

    end

    // UAV l position

    $x_l^{(i)} = v_l \Delta_i \cos(\pi\delta_l^{(i)}/180) + x_l^{(i-1)}$
    $y_l^{(i)} = v_l \Delta_i \sin(\pi\delta_l^{(i)}/180) + y_l^{(i-1)}$;

    // Compute the current SE

    Compute $\mathrm{SE}_k^{(i)}\ \forall k \in \{1, \dots K\}$ by solving (27) and (28) in (9) and (8);

    // Compute the SE difference

    Set $\mathrm{SE}_{\mathrm{diff}}^{(i)} = \frac{1}{K}\sum_{k=1}^{K}\left(\mathrm{SE}_k^{(i)} - \mathrm{SE}_k^{(i-1)}\right)$;

    // Compute variance parameter

    Set $\sigma_\delta^{(i)} = \min\left(\sigma_\delta^{\max}, \frac{1}{\left|\mathrm{SE}_{\mathrm{diff}}^{(i)}\right|}\right)$;

  end

  // Set the UAV l position at iteration that leads to the maximum SE increase

  Set $i^\star = \arg\max_i \sum_{k=1}^{K} \mathrm{SE}_k^{(i)}$;

  Set $[x_l, y_l] = [x_l^{(i^\star)}, y_l^{(i^\star)}]$ as the value of iteration $i^\star$;

end

Output: Updated positions of UAVs: $[x_l, y_l]\ \forall l \in \mathcal{M}_{k^{\min}}$

corresponding to the number of connections in the network [26]. Then, the time complexity of the algorithm can be defined as $\mathcal{O}(\mathrm{n_i} K_s^2 C_{\max} N^3)$, where $K_s = \min(K, K_{\max})$.

V. Numerical Results

This section shows illustrative numerical results of the UC D-mMIMO system enabled by UAVs. The results for the proposed UAV trajectory optimization are presented for scenarios where only aerial TRPs is deployed and also for the case of both aerial and terrestrial TRPs are used.

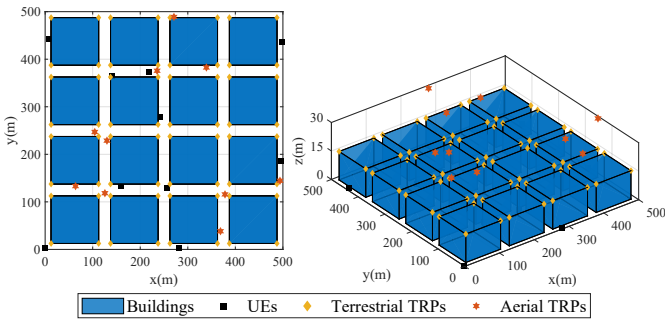

Fig. 4. Considered urban-dense scenario to analyze UC D-mMIMO network enabled by a swarm of UAVs as TRPs. In scenarios containing terrestrial TRPs, they are placed atop the building's edges.

The simulation scenario has a 500 m x 500 m square coverage area, with 16 building blocks of 100 m square length and 15 m high, as depicted in Fig. 4. The grid structure is common in major cities like Barcelona and New York, making it a suitable model for urban-dense environments. The UEs are randomly deployed throughout the streets of the scenario. For scenarios containing terrestrial TRPs, they are located at the top of building edges. Initially, the aerial TRPs are carried by UAVs hovering above the streets at 30 m height. The UAVs positioning and heights can change by performing the proposed trajectory optimization method in Algorithm 1, where the UAVs always flies at heights above the buildings. To determine the presence of a LoS link between each UE and TRP, we check whether the buildings in Fig. 4 physically obstruct the LoS component or not. Table I presents the remaining simulation parameters.

TABLE I
System, channel, and signal simulation parameters.

Parameter	Value
UEs heights	1.65 m
Aerial and terrestrial TRPs heights	30 m and 16.65 m
Receiver noise figure	7 dB
Coherence interval	$\tau_c = 200$ samples
UL pilot length	$\tau_p = 10$ samples
Maximum TRPs per UE	$C_{\max} = 10$
Carrier frequency	$f_c = 3.5$ GHz
Bandwidth	$B = 100$ MHz
TRP's total DL power	$\rho_l = 23$ dBm
UE's total UL power	$\eta_k = 20$ dBm
Angular standard deviations	$\sigma_\varphi = \sigma_\theta = 15^\circ$
ULA antenna spacing	1/2 wavelength distance
Urban environment settings	$a = 9.61$, $b = 0.16$, $\eta^{\mathrm{LoS}} = 1$, $\eta^{\mathrm{NLoS}} = 20$
Continue stationary and come to a halt probabilities	$p_s = 0.15$, $p_h = 0.3$
Time between episodes and iterations	$\Delta_n = 5/v_{\max}$, $\Delta_i = \Delta_n/\mathrm{n_i}$
Variances for UEs and UAVs	$\sigma_\phi = 5$, $\sigma_\delta^{\max} = 30$
Number of setups, episodes, and iterations	$\mathrm{n_s} = 100$, $\mathrm{n_e} = 100$, and $\mathrm{n_i} = 100$

The maximum number of UEs is based on a high-density urban area with 10,000 people per km^2, 25% of them being

outdoor UEs, and the operator has a contract with one-third of outdoor UEs. Three UE density scenarios are simulated to emulate different load behavior. The corresponding number of UEs according to the coverage area is shown in Table II. The presented numbers represent low, medium, and high UE density, which are equivalent to 144, 520, and 800 UEs/km^2, respectively. The number of deployed TRPs depends on the number of UEs, antennas per TRP, and the expected data rate of 200 Mbit/s demand per UE using MR precoding. The procedure to determine the number of deployed TRPs is resumed by computing the average rate R for a given value of L, N, and K, using Monte Carlo simulations. The set of TRP count and achieved rate are stored in sets $\mathcal{L} = \{L_{\min}, L_{\min} + L_{\text{step}}, \cdots, L_{\max}\}$ and $\mathcal{R} = \{R_1, R_2, \cdots, R_{|\mathcal{L}|}\}$, respectively. By noting that $R_1 < R_2 < \cdots < R_{|\mathcal{L}|}$, it is possible to interpolate the results to determine any arbitrary L that leads to an average rate R. To obtain the values at Table II, $L_{\min} = K/\tau_p$ and $L_{\max} = 800$. Since the results are depicted in terms of SE throughout this paper, note that 200 Mbit/s per UE is equivalent to 2 bit/s/Hz with the adoption of 100 MHz bandwidth.

TABLE II
NUMBER OF DEPLOYED TRPS FOR DIFFERENT UE DENSITY SCENARIOS.

UE density	Number of UEs (K)	Number deployed of TRPs (L)	
		N = 2	N = 4
Low	36	84	48
Medium	130	303	167
High	200	491	265

In the distributed implementation, the power coefficients at TRP l are determined as $\rho_{kl} = \rho_d \sqrt{\beta_{kl}} / \sum_{k' \in \mathcal{D}l} \sqrt{\beta_{k'l}}$, where ρ_d represents the maximum transmit power per TRP. The centralized approach adopts scalable fractional power control with the parameters set to $v = -0.5$ and $\kappa = 0.5$ [7]. The EE parameters related to the power consumption of the hardware of the TRPs, and fronthaul links are summarized in Table III, which follows [29], [34]. The DSPs parameters align with Texas Instruments TMS320C6678, and those for GPPs are based on dual Intel Xeon Gold 6338N processors. The remaining parameters used to compute the CC in GOPS are based conventional 5G new radio (NR) with 30 kHz of subcarrier spacing, where $N_{\text{DFT}} = 3300$, $f_s = 122.88$ MHz, and $T_s = 35.38\,\mu$s. The parameters used to model the propulsion power are set as follows: $m_{\text{tot}} = 0.411$ kg, $\eta = 0.7$, $r = 4$, $\rho = 1.225$ kg/m^3, $\varsigma = 0.0176$ m^2, $C_D = 2.49$ and $A = 0.0636$ m^2, and battery capacity of 2.0457×10^5 Joules [36]. To compute fronthaul rate, the number of quantization bits per sample for data transmissions in the distributed implementation and centralized implementation, b_{kl}^d and b_l^d, are computed by incrementing the bit width until an acceptable SE degradation due to fronthaul data samples is achieved, which is set as $a_{\text{deg}} = 0.1$ bit/s/Hz. Moreover, the achievable SE assuming quantization of the bits per sample transmitted over fronthaul links is computed as in [37]. In centralized implementations, the fronthaul rate is computed by setting pilot samples bit width as $b_l^{\text{p}} = 10$.

TABLE III
PARAMETERS ASSUMED FOR CALCULATING THE POWER CONSUMPTION IN CPUS, BACKHAUL/FRONTHAUL LINKS, AND EE.

Parameter	Value	Parameter	Value
$P_{l,0}^{\text{proc}}$, $P_{\text{GPP},0}^{\text{proc}}$	7.3 W, 212.4 W	$P_{0,l}$	0.825 W
Δ_l^{proc}, $\Delta_{\text{GPP}}^{\text{proc}}$	13.64 W, 452.08 W	$P_{\text{ft},l}$	0.25 W/(Gbit/s)
$CC_l^{\max}$	180 GOPS	σ_{cool}, γ_l	0.9, 0.4
$CC_{\text{GPP}}^{\max}$	10777 GOPS	P_{fixed}	450 W

A. 3D Trajectory of UAVs

This subsection delves into cases where UAVs are deployed to provide mobile service coverage when terrestrial infrastructure is unavailable due to malfunctioning, disasters, or when it has not been deployed.

Fig. 5 depicts the average SE of UEs plotted against the episode number. This result is derived from various Monte Carlo independent simulations, with random initial positions assigned to both TRPs and UEs. The analysis assumes MR precoding scheme for different UE density scenarios, as outlined in Table II. The proposed algorithm for UAVs' positions adjustment is compared to the case where their positions remain fixed. It can be observed that when the UAVs are stationary, the SE tends to remain constant throughout the episode steps. This is attributed to the movement of UEs, which can yield both positive and negative impacts on the SE. Since the results are an average of different setups, one effect cancels out the other, leading to a stable average SE. On the other hand, the average SE monotonically increases with the episodes when the proposed algorithm is performed. This demonstrates that UAVs can iteratively adjust their positions to improve SE within each episode, allowing for dynamic adaptation to the UEs movement across episodes.

Moreover, the results in Fig. 5 show that the highest increase in SE of the proposed algorithm are achieved when UE density is lower. For instance, with 2 antennas per TRP, the average SE improvement is 23.75% for low UE density, while reaches only 2.44% in high UE density. Nonetheless, the SE improvement for scenarios with 4 antennas per TRP is slightly better, reaching 29.76% for low UE density and going to 6.56% in scenarios of high UE density. These results suggest that the proposed algorithm yields less SE improvement as more UAVs are deployed, given that results for 2 antennas are slightly worse than for 4 antennas. This occurs because only a limited number of UAVs can modify their positions within each episode. Consequently, with an increased number of deployed UAVs, the fraction of them capable of adjusting their positions reduces, leading to slightly reduced SE improvements.

Fig. 6 presents the average SE of the UEs versus the episode number for the proposed UAV trajectory optimization when the number of iterations n_i varies. The results assume MR precoding for low UE density scenario with 4 antennas per TRP, and evaluate up to 500 episodes. It is observed that the performance of the proposed method improves with an increase in the number of iterations. In episode 500, the SE improvements of the proposed approach compared to the fixed UAV positions reach 38%, 28.6%, and 10.8% for n_i equal to 100, 50, and 10, respectively. It is interesting that even with

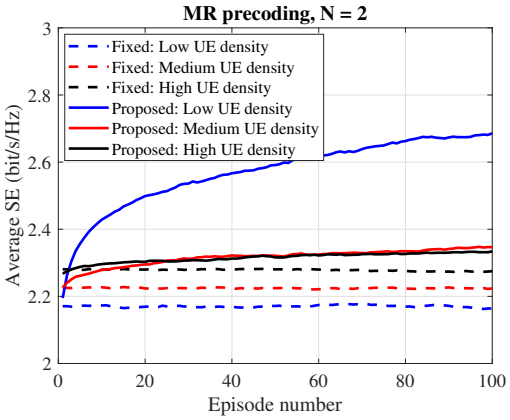

(a) $N = 2$

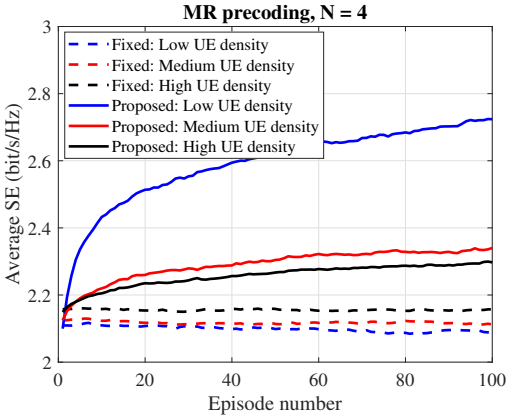

(b) $N = 4$

Fig. 5. Average DL SE of UEs per episode for MR precoding at low, medium, and high UE density scenarios.

the number of iterations as low as 2 and 5 yields slight SE improvements, although it is clear that guaranteeing a higher number of iterations is preferable.

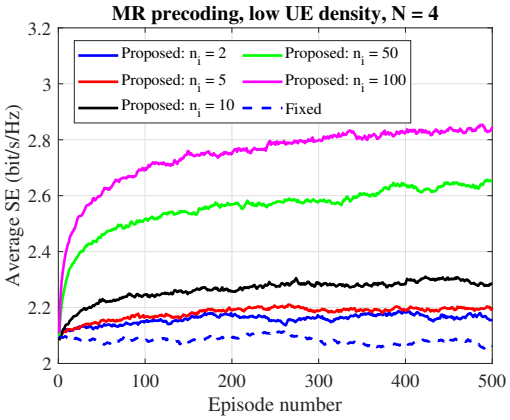

Fig. 6. Average DL SE of UEs per episode for different number of iterations ($\mathrm{n_i}$) in the proposed UAV trajectory optimization. Results consider the low UE density scenario, with $N = 4$ and MR precoding.

Nonetheless, it is important to note that the number of iterations is not always a controllable design parameter. It is computed as the velocity ratio of UAVs and UEs and represents the time frame where UEs positions do not change considerably. In this way, if the UEs velocities are high, it may not be possible to deploy UAVs with even higher velocities. If we assume a maximum UAV velocity of 100 km/h, the allowed UEs velocities depend on the number of iterations $\mathrm{n_i}$. Besides, the required propulsion power of UAVs increases with their velocities, which may lower EE even though SE improves. Fig. 7 illustrates the average DL EE of UEs vs. the maximum UE velocity varying the number of iterations $\mathrm{n_i}$, exemplifying how the UEs and UAVs velocities impact the total EE. The results in this figure assume the average EE performance of the proposed algorithm obtained at episode 100. It can be noted that EE of the proposed algorithm can be lower than the fixed positioning approach, depending on the UEs velocities and number of iterations $\mathrm{n_i}$. For instance, with a maximum UE velocity of 20 km/h, the SE gains provided by a five-fold higher UAV velocity (i.e., $\mathrm{n_i} = 5$) do not compensate in terms of EE compared with fixed positioning.

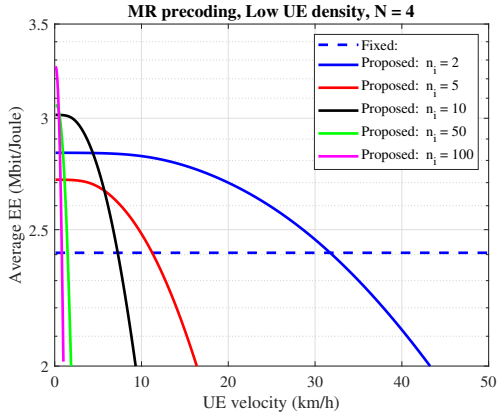

Fig. 7. Average DL EE of UEs vs. maximum velocity of UEs varying the number of iterations $\mathrm{n_i}$. Results are for MR precoding, low UE density, with $N = 4$.

Moreover, the intersection points where the proposed approach matches the fixed positions occur at even lower UE speeds the higher the $\mathrm{n_i}$ value, as shown in Fig. 7. This portrays the dominance of the UAVs propulsion power over the other variables in the total power consumption, especially at higher UAVs speeds. In terms of flight autonomy, the impact of the increased power consumption for high UAV speeds affects the just UAVs that are adjusting their positions. Since the proposed method alternates the selected UAVs in each episode, the reduction of flight autonomy time of each UAV is mitigated. Essentially, each UAV moves at a higher speed for a brief period before hovering and allowing the next UAV to move. For example, if we consider a maximum speed of 10 km/m for the UEs, we can determine the flight autonomy time by varying the maximum speed of the UAV. Additional results show that with a maximum UAV velocity of 20 km/m (when $\mathrm{n_i} = 2$), the flight autonomy time is around 51 minutes. Similarly, with a maximum UAV velocity of 100 km/m (when $\mathrm{n_i} = 10$), the flight autonomy time reduces to 46 minutes. This time difference is not significant because the UAVs alternate between moving and hovering.

Fig. 8 illustrates the performance of the proposed UAV trajectory optimization for MR, LP-MMSE, P-RZF, and

P-MMSE precoding schemes. Results consider low UE density scenarios. Noticeable, the algorithm to heuristically optimize the UAV positions can be used with precoding schemes other than MR, even though it is based on the simpler MR closed-form expressions for achievable SE. Recall that the proposed algorithm uses the MR closed-form regardless of the precoding choice to take advantage of the long-term CSI.

Furthermore, the findings depicted in Fig. 8 provide evidence of the superior performance of distributed LP-MMSE, centralized P-RZF and P-MMSE compared to MR. For instance, their average SE can exceed that of MR by more than twofold (approximately 2.17 to 2.41 times higher). Besides, the SE improvements achieved by the proposed approach are also higher, e.g., up to 47.84% for LP-MMSE, 38.14% for P-RZF, and 35.24% for P-MMSE, when compared with the fixed UAV position with 4 antennas per TRP. As with MR precoding, the results for the other precoding schemes also show that the 4 antennas per TRP configuration yields slightly higher SE improvements than with 2 antennas per TRP, although not readily observable in the figure. An interesting behavior to notice is that LP-MMSE favors the 4 antennas per TRP scenario while P-RZF and P-MMSE perform better with 4 antennas. This is attributed to the impact of the number of antennas per TRP in their capacity to mitigate interference. Generally, centralized precoding schemes are able to combine information of different TRPs to mitigate better inference, benefiting from having more TRPs across the coverage area. On the other hand, distributed precoding uses only local information, requiring a balance in the number of TRPs and antennas per TRP.

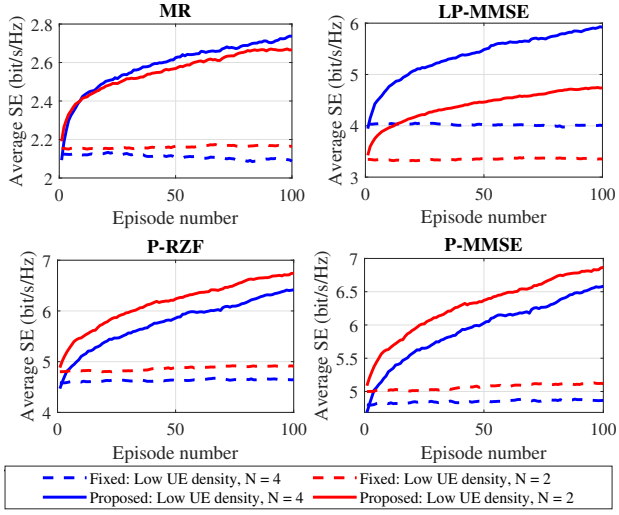

Fig. 8. Average DL SE of UEs per episode for MR, LP-MMSE, P-RZF, and P-MMSE precoding schemes. Results consider low UE density scenarios.

B. Hybrid Terrestrial and Aerial TRPs Scenario

This subsection explores scenarios where UAVs are temporarily deployed to assist in cases where the terrestrial infrastructure is still available, but a surge in demand requires additional TRPs to provide a better service experience. Specifically, hybrid scenarios that combine aerial and terrestrial TRPs are evaluated to deal with high UE density traffic and high UEs data rates demands. It is assumed the path loss and LoS probability models for both terrestrial and aerial TRPs remain consistent, mitigating potential influences on the following result evaluation.

Fig. 9 illustrates the average DL SE of UEs per episode for medium and high UE density and $N = 4$. The results compare D-mMIMO systems consisting exclusively of terrestrial TRPs with those with a combination of terrestrial and aerial TRPs. It also presents results for MR, LP-MMSE, P-RZF, and P-MMSE precoding schemes. In the results, L_t stands for the number of terrestrial TRPs while L_a stands for the number of aerial TRPs, with the total number of TRPs defined as $L = L_t + L_a$. The simulation parameters emulate scenarios where the terrestrial infrastructure is deployed to serve a medium UE density (i.e., $K = 130$, $L = L_t = 167$). For instance, this provides an average SE per UE of 2.275 bit/s/Hz with MR precoding. However, when the number of UEs increases (high UE density with $K = 200$), the deployed terrestrial TRP can only provide 1.817 bit/s/Hz per UE. This represents a decrease of approximately 20% due to the increased interference and competition for radio resources. Fortunately, with the aid of UAVs, it is possible to restore the per UE performance to 2.144 bit/s/Hz if $L_a = 49$ or up to 2.359 bit/s/Hz if $L_a = 98$. In the LP-MMSE, P-RZF, and P-MMSE precoding schemes, similar behaviors can be observed. However, even after deploying an additional 98 UAVs when the number of UEs is 200, the SE performance is not superior to that of the terrestrial scenario with only 130 UEs, as it happens with MR precoding. To achieve that, these precoding options would require even more additional TRPs, especially in the case of LP-MMSE. Nonetheless, these precoding choices provide superior performance than MR in any of the analyzed cases. Additionally, P-MMSE precoding is the one that achieves the highest SE performance, making it the preferable choice.

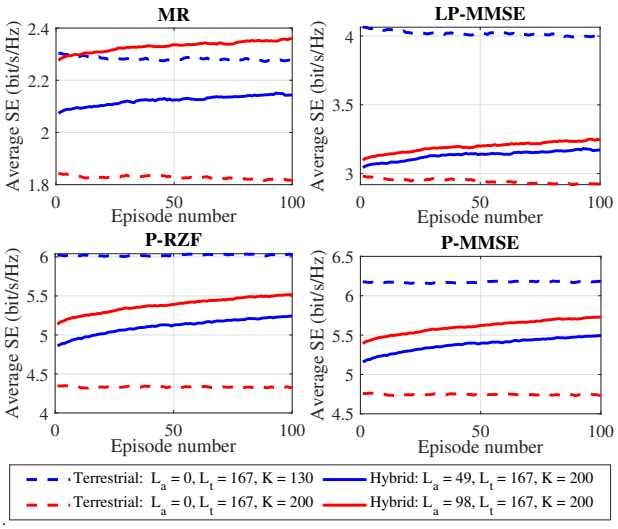

Fig. 9. Average DL SE of UEs per episode for medium and high UE density and $N = 4$. Comparison between D-mMIMO systems consisting exclusively of terrestrial TRPs and those with a combination of terrestrial and aerial TRPs. Results are for MR, LP-MMSE, P-RZF, and P-MMSE precoding schemes.

C. Required Fronthaul Rate

This section investigates the required rate of the wireless fronthaul links connecting the TRPs to the CPU. In Fig. 10, the results consider UC D-mMIMO systems consisting exclusively of aerial TRPs UAVs, for a low UE density scenarios, when the proposed UAV trajectory optimization is performed.

Fig. 10a presents the required fronthaul rate for distributed LP-MMSE and centralized P-MMSE precoding schemes. For both precoding schemes, the required fronthaul rate increases with the number of antennas per TRP. This occurs because the achievable UEs' SE also increases with the number of antennas per TRP. Hence, in order to maintain an acceptable SE degradation due to fronthaul data samples set as $a_{\text{deg}} = 0.1$ bit/s/Hz, the bit width also increases. Furthermore, it is noteworthy that the required fronthaul rate is much higher for a distributed implementation than for a centralized one. For $N = 2$ and $N = 4$, the rate can be around 2.7 and 1.9 times higher, respectively, when comparing distributed to centralized implementations. This happens because the fronthaul rate scales with different parameters, as exposed in (24). In distributed implantation, it scales with the number of UEs served by each TRP, which is set as $|\mathcal{D}_l| \leq (\tau_p = 10)$. Whereas in centralized implementations, it scales with the number of antennas per TRP N, which in the results is set either as 2 or 4. Noting that $N \leq \tau_p$, this behavior is expected.

In Fig. 10b, it is shown the cumulative distribution function (CDF) of DL SE with and without a maximum fronthaul rate per link constraint. If a maximum fronthaul rate per TRP is assumed, the number of quantization bits per sample for data transmissions is still computed by incrementing the bit width to achieve an acceptable SE degradation of $a_{\text{deg}} = 0.1$ bit/s/Hz, but only up to a maximum bit width value. In the results, the maximum bit width value corresponds to a rate of 10 Gbit/s, which is computed using (24). The results analyze only LP-MMSE precoding since it can require more than 10 Gbit/s per link when there is no fronthaul rate limitation, as shown in Fig. 10a. It can be noticed that limiting the fronthaul rate to 10 Gbit/s has little impact on the CDF of SE. Only the most fortunate UEs suffer a slight decrease in their SE performances.

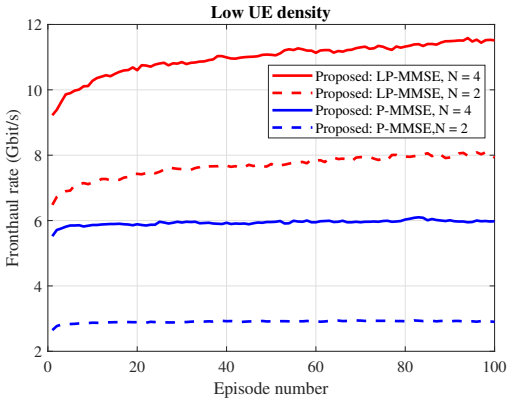

(a) Fronthaul rate

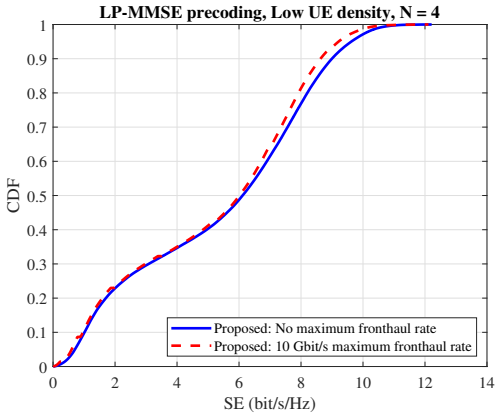

(b) CDF of DL SE

Fig. 10. (a) Average required fronthaul rate per episode for LP-MMSE and P-MMSE precoding schemes. (b) CDF of DL SE with and without limitation of the fronthaul rate. Both results are shown for low UE density scenarios.

VI. Conclusions

This paper investigated the performance of scalable UC D-mMIMO systems enabled by a swarm of UAVs acting as TRPs, which could operate independently or in conjunction with terrestrial TRPs. A comprehensive study on deployment and trajectory optimization of UAVs was conducted, proposing a novel heuristic approach to optimize the positions of aerial TRPs. As far as the authors are aware of, the proposed heuristic approach is the first to consider the continuous movement of UEs within the coverage area for UC D-mMIMO systems. Specifically, it optimizes the three-dimensional locations of each UAV under a time-discretized framework divided into episodes, each consisting of several iterations. The positions of UEs vary between episodes through a discrete-time Markov chain. The positions of TRPs are optimized iteratively based on the ratio between maximum velocities of UAVs and UEs, and the MR precoding closed form for SE. Moreover, each UAV adjusts its position independently, guaranteeing the SE is not affected by the movements of other UAVs.

The evaluation of the heuristic approach assessed the achievable DL SE performance using MR, LP-MMSE, P-RZF, and P-MMSE precoding, assuming densities from 144 to 800 UEs per km^2. Results indicated that although the optimization only utilizes the MR equations, the method can be applied to more advanced precoding with significant performance improvements for all considered UE densities. In fact, for a fully aerial network with low UE density, the SE enhancements were 29.76% for MR, 47.84% for LP-MMSE, 38.14% for P-RZF, and 35.24% for P-MMSE, comparing the proposed method with fixed UAV deployment. The most significant SE improvements were usually found at the lower UE density and with a higher number of iterations. Despite this, in terms of DL EE, the additional propulsion power required for UAVs to move at high speeds may not be justified by the benefits of more iterations.

Another notable insight from the results was that when the terrestrial infrastructure is overwhelmed by a surge in UE density or demand, temporarily deploying UAVs can restore network performance in terms of SE. Finally, the effects of fronthaul constraints were also examined. Specifically, when

the fronthaul rate was limited to 10 Gbit/s, it had no significant impact on the CDF of SE compared to scenarios with unconstrained fronthaul. Additionally, when seeking a quantization level with minimal SE degradation under unrestricted fronthaul rates, the findings indicated that LP-MMSE distributed precoding require more fronthaul capacity than centralized options.

Based on the observed findings and novelty of the proposed approach, it is reasonable to suggest that this paper can serve as a benchmark for subsequent studies in this field. Future research directions might include exploring the use of fixed-wing UAVs within the proposed framework, and examining the effects of channel aging, which leads channel estimates to become rapidly outdated due to the mobility of both UEs and UAVs. Further investigations could also assess different antenna array configurations and patterns, evaluate how weather conditions affect UAVs' positioning accuracy, and consider the implications of no-fly zones that restrict the operational spaces of UAVs.

ACKNOWLEDGMENT

This study was granted access to the computational resources of the High Performance Computer Center (https://www.ccad.ufpa.br/) at the Federal University of Pará.

REFERENCES

[1] J. Zhang, S. Chen, Y. Lin, J. Zheng, B. Ai, and L. Hanzo, "Cell-free massive MIMO: A new next-generation paradigm," *IEEE Access*, vol. 7, pp. 99 878–99 888, Jul. 2019.

[2] J. Zhang, E. Björnson, M. Matthaiou, D. W. K. Ng, H. Yang, and D. J. Love, "Prospective multiple antenna technologies for beyond 5G," *IEEE J. Sel. Areas Commun.*, vol. 38, no. 8, pp. 1637–1660, Aug. 2020.

[3] G. Interdonato, E. Björnson, H. Q. Ngo, P. K. Frenger, and E. G. Larsson, "Ubiquitous cell-free massive MIMO communications," *EURASIP J. Wirel. Commun. Netw.*, vol. 2019, p. 197, Aug. 2019.

[4] H. Q. Ngo, A. Ashikhmin, H. Yang, E. G. Larsson, and T. L. Marzetta, "Cell-free massive MIMO versus small cells," *IEEE Trans. Wireless Commun.*, vol. 16, no. 3, pp. 1834–1850, Mar. 2017.

[5] E. Björnson and L. Sanguinetti, "Scalable cell-free massive MIMO systems," *IEEE Trans. Commun.*, vol. 68, no. 7, pp. 4247–4261, Jul. 2020.

[6] E. Björnson and L. Sanguinetti, "Making cell-free massive MIMO competitive with MMSE processing and centralized implementation," *IEEE Trans. Wireless Commun.*, vol. 19, no. 1, pp. 77–90, Jan. 2019.

[7] Ö. Demir, E. Björnson, and L. Sanguinetti, *Foundations of User-Centric Cell-Free Massive MIMO*. Foundations and Trends in Signal Processing Series, Now Publishers, 2021.

[8] W. Shin and M. Vaezi, *UAV-Enabled Cellular Networks*. Cham: Springer International Publishing, 2021, pp. 165–200.

[9] "Handbook of unmanned aerial vehicles," 2015. [Online]. Available: http://dx.doi.org/10.1007/978-90-481-9707-1

[10] A. A. Khalil, M. Y. Selim, and M. A. Rahman, "CURE: Enabling RF energy harvesting using cell-free massive MIMO UAVs assisted by RIS," in *2021 IEEE LCN*, Oct. 2021, pp. 533–540.

[11] O. Abbasi and H. Yanikomeroglu, "A cell-free scheme for UAV base stations with HAPS-assisted backhauling in terahertz band," in *Proc. IEEE Int. Conf. Commun. (ICC)*, May 2022, pp. 249–254.

[12] L. Wang and Q. Zhang, "Cell-free massive MIMO with UAV access points: UAV location optimization," in *Proc. IEEE/CIC Intern. Conf. Commun. in China (ICCC)*, Aug. 2022, pp. 262–267.

[13] C. Diaz-Vilor, A. Lozano, and H. Jafarkhani, "Cell-free UAV networks: Asymptotic analysis and deployment optimization," *IEEE Trans. Wireless Commun.*, pp. 1–1, May 2022.

[14] ——, "Cell-free UAV networks with wireless fronthaul: Analysis and optimization," *IEEE Trans. Wireless Commun.*, vol. 23, no. 3, pp. 2054–2069, 2024.

[15] A. Ahmed, C. Chaieb, W. Ajib, H. Elbiaze, and R. Glitho, "Resource allocation and UAVs placement in cell-free wireless networks," in *Proc. IEEE Global Commun. Conf.*, Dec. 2022, pp. 5995–6000.

[16] C. Liu, W. Feng, Y. Chen, C.-X. Wang, and N. Ge, "Cell-free satellite-UAV networks for 6G wide-area internet of things," *IEEE J. Sel. Areas Commun.*, vol. 39, no. 4, pp. 1116–1131, Apr. 2021.

[17] Z. Wu and Q. Wang, "Trajectory optimization and power allocation for cell-free satellite-UAV internet of things," *IEEE Access*, vol. 11, pp. 203–213, 2023.

[18] Y. K. Tun, Y. M. Park, T. H. T. Le, Z. Han, and C. S. Hong, "A business model for resource sharing in cell-free UAVs-assisted wireless networks," *IEEE Trans. Veh. Technol.*, vol. 71, no. 8, pp. 8839–8852, Aug. 2022.

[19] M. Samir, D. Ebrahimi, C. Assi, S. Sharafeddine, and A. Ghrayeb, "Leveraging UAVs for coverage in cell-free vehicular networks: A deep reinforcement learning approach," *IEEE Trans. Mobile Comput.*, vol. 20, no. 9, pp. 2835–2847, Sep. 2021.

[20] Y. Chen, X. Zhang, F. Yao, K. An, G. Zheng, and S. Chatzinotas, "Pilot assignment and power control in secure UAV-enabled cell-free massive MIMO networks," *IEEE Internet of Things J.*, vol. 11, no. 2, pp. 3377–3391, 2024.

[21] C. D'Andrea, A. Garcia-Rodriguez, G. Geraci, L. G. Giordano, and S. Buzzi, "Cell-free massive MIMO for UAV communications," in *Proc. IEEE Int. Conf. Commun. Workshops*, May 2019, pp. 1–6.

[22] S.-N. Jin, D.-W. Yue, and H. H. Nguyen, "Spectral and energy efficiency in cell-free massive MIMO systems over correlated Rician fading," *IEEE Systems Journal*, vol. 15, no. 2, pp. 2822–2833, Jun. 2021.

[23] A. A. Polegre, F. Riera-Palou, G. Femenias, and A. G. Armada, "Channel hardening in cell-free and user-centric massive MIMO networks with spatially correlated Ricean fading," *IEEE Access*, vol. 8, pp. 139 827–139 845, 2020.

[24] O. Özdogan, E. Björnson, and E. G. Larsson, "Massive MIMO with spatially correlated Rician fading channels," *IEEE Trans. Commun.*, vol. 67, no. 5, pp. 3234–3250, May 2019.

[25] A. Al-Hourani, S. Kandeepan, and S. Lardner, "Optimal LAP altitude for maximum coverage," *IEEE Wireless Commun. Lett.*, vol. 3, no. 6, pp. 569–572, Dec. 2014.

[26] M. M. M. Freitas, D. D. Souza, A. L. P. Fernandes, D. B. da Costa, A. M. Cavalcante, L. Valcarenghi, and J. C. W. A. Costa, "Scalable user-centric distributed massive MIMO systems with limited processing capacity," in *Proc. IEEE Int. Conf. Commun. (ICC)*, 2023, pp. 1–7.

[27] D. D. Souza, M. M. M. Freitas, D. B. da Costa, G. S. Borges, A. M. Cavalcante, L. Valcarenghi, and J. C. Weyl Albuquerque Costa, "Effective channel DL pilot-based estimation in user-centric cell-free massive MIMO networks," in *Proc. IEEE Global Commun. Conf.*, Dec. 2022, pp. 705–710.

[28] E. Björnson, J. Hoydis, and L. Sanguinetti, *Massive MIMO Networks: Spectral, Energy, and Hardware Efficiency*. Foundations and Trends in Signal Processing Series, Now Publishers, 2018.

[29] O. T. Demir, M. Masoudi, E. Björnson, and C. Cavdar, "Cell-free massive MIMO in O-RAN: Energy-aware joint orchestration of cloud, fronthaul, and radio resources," *IEEE J. Sel. Areas Commun.*, Jan. 2024.

[30] S. Malkowsky *et al.*, "The world's first real-time testbed for massive MIMO: Design, implementation, and validation," *IEEE Access*, vol. 5, pp. 9073–9088, 2017.

[31] C. Desset and B. Debaillie, "Massive MIMO for energy-efficient communications," in *Proc. European Microwave Conference (EuMC)*, Oct. 2016, pp. 138–141.

[32] B. Debaillie, C. Desset, and F. Louagie, "A flexible and future-proof power model for cellular base stations," in *Proc. IEEE VTC Spring*, May 2015, pp. 1–7.

[33] E. Björnson, L. Sanguinetti, J. Hoydis, and M. Debbah, "Optimal design of energy-efficient multi-user MIMO systems: Is massive MIMO the answer?" *IEEE Trans. Wireless Commun*, vol. 14, no. 6, pp. 3059–3075, Jun. 2015.

[34] H. Q. Ngo, L. Tran, T. Q. Duong, M. Matthaiou, and E. G. Larsson, "On the total energy efficiency of cell-free massive MIMO," *IEEE Trans. Green Commun. Netw*, vol. 2, no. 1, pp. 25–39, Mar. 2018.

[35] K. Dorling, J. Heinrichs, G. G. Messier, and S. Magierowski, "Vehicle routing problems for drone delivery," *IEEE Trans. Syst., Man, Cybern.: Syst.*, vol. 47, no. 1, pp. 70–85, Jan. 2017.

[36] J. Zhang, J. F. Campbell, D. C. Sweeney II, and A. C. Hupman, "Energy consumption models for delivery drones: A comparison and assessment," *Transp. Res. Part D: Transp. Environ.*, vol. 90, p. 102668, Jan. 2021.

[37] G. Femenias and F. Riera-Palou, "Fronthaul-constrained cell-free massive MIMO with low resolution ADCs," *IEEE Access*, vol. 8, pp. 116 195–116 215, Jun. 2020.

[38] O. Özdogan, E. Björnson, and J. Zhang, "Performance of cell-free massive MIMO with Rician fading and phase shifts," *IEEE Trans. Wireless Commun.*, vol. 18, no. 11, p. 5299–5315, Nov. 2019.